

Article

Microscopic Imaging on Diesel Spray and Atomization Process

Yassine El Marnissi ¹ and Joonsik Hwang ^{1,2,3,*}

¹ Department of Mechanical Engineering, Mississippi State University, Starkville, MS 39762, USA; ye44@msstate.edu

² Center for Advanced Vehicular Systems (CAVS), Mississippi State University, Starkville, MS 39759, USA

³ Institute for Clean Energy Technology (ICET), Mississippi State University, Starkville, MS 39759, USA

* Correspondence: hwang@me.msstate.edu

Abstract: Improving diesel engine performance requires a comprehensive understanding of fuel atomization and air–fuel mixing within the combustion chamber. Numerous studies have been conducted to reduce emissions and enhance diesel engines. However, further investigation is required on the detailed diesel spray process. In this study, we adopted extinction measurement to analyze the effects of a fuel injection pressure range of 300 to 700 bar on spray morphology. For the extinction imaging setup, we utilized a high-intensity continuous LED source along with a diffuser to ensure uniform light distribution. The high-speed extinction and image processing results indicate that increasing the injection pressure from 300 to 700 bar effectively produced a smaller particulate size (15% reduction) and a better air–fuel mixing process. Especially at the end of injection, our results show smaller liquid ligaments (50% reduction) and droplets around the injector tip with higher injection pressure cases.

Keywords: atomization; diesel; extinction; mixing; spray

1. Introduction

Detailed measurements of spray characteristics are essential for developing a better understanding and prediction of the dynamics involved in diesel fuel atomization. In pursuit of this understanding, numerous experimental studies have investigated the impacts of injection pressure on specific spray characteristics [1–3]. Despite significant progress in optical techniques, the analysis of spray characteristics and the precise optimization of injection systems for maximum efficiency remain challenging. Numerical investigations on spray atomization have also been conducted to comprehensively understand how the injection pressure affects the spray characteristics in CI engines [4,5]. These studies have proven the prediction capability of spray atomization, which plays a vital role in combustion efficiency. Moreover, the viscosity and surface tension, which are the physical properties of the fuel, as well as the fuel temperature, have been found to significantly influence the spray atomization [6,7]. It is also shown that the formation of fine droplets was achieved through an increase in temperature and a decrease in both viscosity and surface tension. At higher injection pressures, droplets broke up more rapidly in the downstream zone, leading to wider spray dispersion [8,9]. Garai et al. [10] studied the microscopic characteristics of a diesel spray using a hybrid atomizer. They employed particle droplet image analysis (PDIA) to measure the Sauter mean diameter (SMD). They found that increasing the airflow rates resulted in a quicker breakup, which can be attributed to the turbulent nature of the flow, characterized by high Reynolds numbers.

The fuel–air mixture process is significantly influenced by the spray cone angle, which is precisely defined as the angle formed between two lines tangent to the spray, both originating from the nozzle tip. Agarwal et al. [11] investigated the impact of ambient pressure on the cone angle in a constant-volume chamber. Their research revealed an increase in droplet density attributed to the shear resistance generated at higher pressures.



Citation: El Marnissi, Y.; Hwang, J. Microscopic Imaging on Diesel Spray and Atomization Process. *Processes* **2024**, *12*, 359. <https://doi.org/10.3390/pr12020359>

Academic Editor: Jiaqiang E

Received: 14 November 2023

Revised: 23 January 2024

Accepted: 5 February 2024

Published: 8 February 2024



Copyright: © 2024 by the authors. Licensee MDPI, Basel, Switzerland. This article is an open access article distributed under the terms and conditions of the Creative Commons Attribution (CC BY) license (<https://creativecommons.org/licenses/by/4.0/>).

Additionally, Rashid et al. [12] investigated the relationship between injection pressure, inlet slot number, and cone angle. The fuels were injected at injection pressures within a range of 2–8 bar, and the number of inlet slots ranged from 2 to 5. They reported that the spray cone angle is independent of the inlet slot number and increases with higher injection pressure. A study by Nagoaka et al. [13] investigated the influence of nozzle geometry on atomization. Their results showed that as the nozzle length/diameter (L/D) ratio increases, cavitation at the valve-covered orifice (VCO) and mini-sac (MS) nozzles decreases. For a more in-depth insight into droplet size distributions and spray penetration, they employed computational fluid dynamics (CFD). The predicted SMD and spray penetration obtained by simulations agree well with the experimental results.

On the other hand, K.S. Varde [14] found that an increase in injection pressure leads to the introduction of more turbulence into the orifice, causing a decrease in the spray. In particular, the spray cone angle increases as the injection pressure increases for nozzles with low L/D ratios. In contrast, a higher injection pressure often results in a smaller spray cone angle for nozzles with greater L/D ratios. After the L/D ratio reaches a critical value (about $L/D = 4$), the spray cone angle hardly responds to changes in injection pressure. The design of the nozzle orifice and the operational parameters have a significant influence on fuel spray characteristics. Understanding the behavior of these parameters is of significant importance to find a correlation between the spray cone angle and injection pressure. Sovani et al. [15] investigated the impact of the cone angle for a pressure range of 0.27–5.5 MPa. They found that the half cone angle increases linearly as the pressure and gas-to-liquid ratio (GLR) increase at all ambient pressures. Moreover, this study also revealed that the cone angle varies with ambient pressure; it decreases from 0.27 to 1.5 MPa and then increases from 1.5 and 5.5 MPa, which indicates a change in the flow regime within the exit orifice of the injector that is attributed to the non-linear dependency on ambient pressures and to the subsequent unchoking at higher pressures. In a separate study by Jia et al. [16], a 1.14° increase in the cone angle of a diesel spray with the increase in the injection pressure from 100 to 300 MPa was reported, attributed to the turbulence intensity that influences the cavity formation within the orifice. It should also be noted that establishing the characteristics of a diesel spray involves the measurement of core length [17,18]. Turner et al. [19] utilized image processing to measure the variation in core length. They observed that the core length decreases with higher injection pressure. Agarwal et al. [20] studied the influence of the nozzle surface on the atomization of a liquid jet. They analyzed three spray configurations: unprocessed, educated, and purely external flow. Using non-dimensional parameters such as Reynolds, Weber, and Ohnesorge numbers, they found that the unprocessed geometry exhibits larger surface features compared to the educated configuration, which leads to a shorter intact core length. On the other hand, the purely external flow configuration results in a larger core length due to surface disturbances. Meanwhile, according to the study by Kulkarni et al. [21], the intact core length was affected by surface tension. It was found that increasing the gas pressure from 500 mbar to 2000 mbar resulted in shorter intact core lengths due to the aerodynamic forces that enhanced breakup and surmounted the surface tension. Beale et al. [22] focused on the primary and secondary break-up of the intact core length using the Kelvin–Helmholtz (KH) and Rayleigh–Taylor (RT) models. They found that the RT accelerative instabilities influenced the droplets surrounding the liquid core. Even though previous studies have contributed to a certain degree of understanding of the effect of injection pressure on atomization, cone angle, and intact core length, several aspects of spray characteristics, such as dribbling, require further investigation.

An early microscopy imaging study [23] studied the influence of the injection pressure on ligament formation across the entire injection process. Roth et al. [24] utilized the exciplex laser-induced fluorescence LIF method to study liquid jet disintegration at different injection pressures. They found that instabilities, such as oscillations and perturbations, cause the incident liquid to break up into large ligaments. In addition, the needle closing rate can be an additional influential factor. Moon et al. [25] focused on evaluating the fuel cavitation

inside the nozzle. They found that faster flow injection at the needle results in an increase in fuel cavitation. Suh et al. [26] found that a diesel spray with more ligaments, resulting from higher turbulence, enhanced the fuel–air mixture. Koci et al. [27] investigated fuel dribbling in heavy-duty diesel engines using computational fluid dynamics (CFD). Their results showed that fuel injector dribble significantly contributes to unburned hydrocarbons, with a ratio approximately ranging from ~75% to 90% emissions. Pos et al. [28] investigated the microscopic spray characteristics in a multi-hole injector using high-speed imaging to capture the fuel sprays pre- and post-injection. Their results demonstrated that the release of liquid fuel occurs randomly after the end of injection, and the amount released is not related to the injector mileage. Despite these efforts, the spray behavior under different injection pressures still needs to be fully clarified.

This study investigates the effect of injection pressure on diesel spray characteristics (spray tip penetration, spray cone angle, droplet size, intact core length, and ligament). Unlike previous studies that relied on Mie scattering and arbitrary thresholding, which are inaccurate and provide only qualitative data, our study employed extinction imaging and the projected liquid volume (PLV) to offer a more accurate and quantitative analysis of spray behavior. The precise measurements obtained through this study will offer valuable quantitative data for computational fluid dynamics (CFD) model simulations and validation.

2. Experimental Setup and Procedure

Figure 1 presents a schematic diagram illustrating the microscopic spray investigation setup. The chamber, constructed from carbon steel (S45C), had a volume of 1400 cm³ and a cube-shaped design. Two of its sides were equipped with 9.6 cm quartz windows for high-speed imaging, while the remaining four sides were covered with dummy plates. The spray experiments were conducted using a common-rail direct injection system. The injection pressure and quantity were meticulously controlled through a common-rail engine controller (Zenobalti, ZB-9013). We employed a 3-hole Bosch CRI 3.1 piezoelectric injector with a spray hole diameter of 100 µm for these experiments. To ensure precision, we covered all but one hole of the injector nozzle with an injector cap, diverting the sprays from the other two holes to a bypass passage. For high-quality microscopic spray imaging, we utilized a high-intensity continuous light-emitting diode (LED) source. The capturing of near-nozzle flow images was achieved through the use of a high-speed digital video camera (Vision Research Inc., Phantom V.2640) equipped with a long-distance microscope (LDM) lens. The camera was synchronized with the fuel injection system to ensure precise timing, operating at shutter speeds of 190,000 frames per second (fps). Although the initial image resolution was 128 pixels by 64 pixels, we significantly enhanced it to 2551 pixels by 1271 pixels using a super-resolution algorithm [29]. During the spray experiments, we systematically varied the injection pressure within the range of 300 to 700 bar under ambient pressures of 0.1 MPa, while maintaining a constant ambient temperature of 300 K.

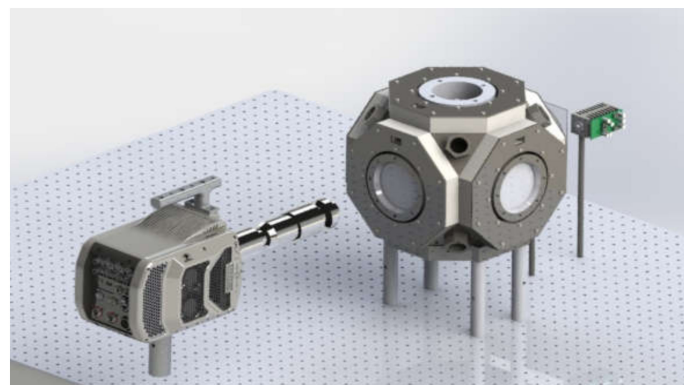


Figure 1. Microscopic spray imaging setup.

3. Image Processing Method

Extinction imaging was used in this experimental analysis. This method provides accurate quantitative information about the concentration of liquid fuel compared to other methods, such as Mie scattering, which measures only the dispersed light intensity. Extinction imaging, alongside diffused backlighting, can effectively measure optical thickness. The optical thickness τ is obtained by using the Beer–Lambert law equation:

$$\tau = -\ln\left(\frac{I}{I_0}\right) \quad (1)$$

where I is the intensity of the transmitted light influenced by droplet extinction and I_0 refers to the incident light. Also note that the optical thickness τ is related to the projected liquid volume (PLV). To calculate PLV, we integrated the liquid volume fraction (LVF) along the cross-stream direction (y), assuming a uniform droplet diameter (d) and extinction coefficient (C_{ext}) along the line of sight. This calculation is based on the optical thickness measurement using Mie scattering and extinction theory.

$$PLV = \tau \frac{\pi d^3 / 6}{C_{ext}} = \int_{-y_\infty}^{y_\infty} (LVF) \cdot dy \quad (2)$$

According to Equation (2), PLV depends on the droplet diameter and extinction coefficient. In our use of Mie theory relations and experimental measurements, we found that the diameter and extinction coefficient were $9 \mu\text{m}$ and $254 \times 10^{-6} \text{mm}^2$, respectively. A threshold value of $0.2 \cdot 10^{-3} \text{mm}^3 (\text{liquid})/\text{mm}^2$ was used when processing the PLV images. It should also be noted that using computational fluid dynamics (CFD) simulations can be useful for calculating the PLV, which can then be compared to the experimental measurements. The spray characteristics presented in this study represent the average values derived from three experimental runs. The error bars represent the standard error ($\pm\sigma/\sqrt{n}$) for the intact core, droplet size, and ligaments, respectively.

4. Spray Images Analysis

Spray images were captured using a high-speed camera and extinction imaging techniques.

At each injection pressure, 500 images were captured to collect information about liquid structures. A total of 2500 images were processed with the MATLAB toolbox. The first step in image processing was to apply background subtraction to isolate the spray from its background. Then, we binarized the resulting images using a threshold to create a binary mask, assigning pixel values of 0 for black and 255 for white. Figure 2 defines two key spray characteristics: spray tip penetration and cone angle. Spray tip penetration is defined as the distance from the spray nozzle to the farthest point of the spray boundary. This distance was calculated using the Euclidean distance formula. The cone angle is represented as the angle formed between two tangential lines at the nozzle spray boundary (illustrated by the red lines in Figure 3c). The MATLAB 2022b functions ‘`imfindcircles`’ and ‘`regionprops`’ were used for microscopic analysis to detect droplets and find their average sizes. It is important to note that the measurement techniques used were a combination of functions that detect the center and the size of the droplet. Furthermore, ligaments (elongated liquid structures) were also measured using boundary detection techniques to measure their size accurately.

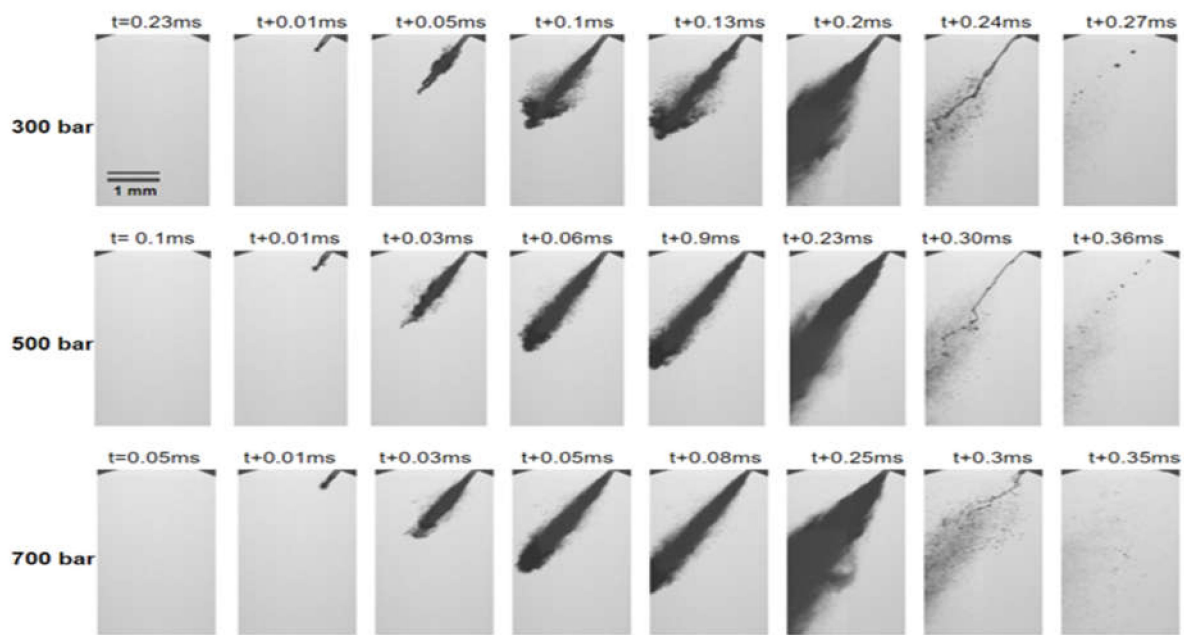


Figure 2. Diesel spray development under varying injection pressures.

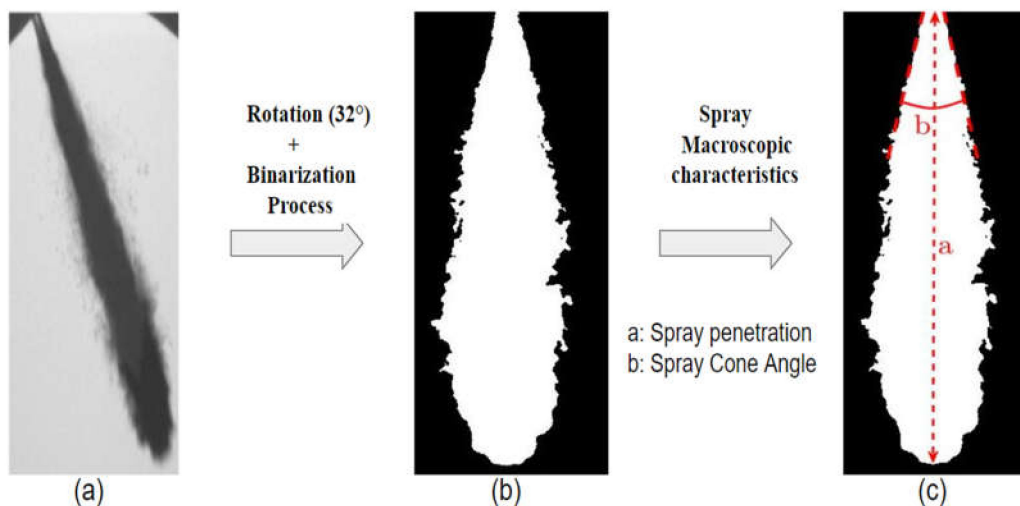


Figure 3. Image processing for diesel spray analysis. (a) Raw image. (b) Binarizing the image. (c) Macroscopic spray parameters.

5. Temporal Evolution Analysis of a Diesel Spray

The main focus of this study was to investigate the behavior of a diesel spray under varying injection pressures. In this experiment, the injection duration was maintained at 0.55 ms. We recorded a delay after the start of injection, which varied depending on the injection pressure: 0.23 ms at 300 bar, 0.15 ms at 400 bar, 0.065 ms at 600 bar, and 0.05 ms at 700 bar.

To ensure accuracy in the measurement of spray characteristics, we employed PDE-based interpolation methods to produce sharper edges by integrating texture enhancement as a post-process. This post-process resulted in a super-resolution interpolator (SRI), which restored sharp features and improved microscopic structures. Macroscopic characteristics such as penetration, cone angle, and core length were observed during the initial, transient, and turbulent injection stages, while microscopic features became more noticeable towards the end of the injection process, as the high turbulence and optical thickness during the main injection restricted the extraction of ligament and droplet information. The optical

setup in this study enabled us to monitor the microscopic characteristics, offering valuable insights into the end of the injection process.

6. Results and Discussion

The results and discussion of this paper are divided into two main sections to understand the effects of injection pressure on spray characteristics. The first section studies the macroscopic characteristics, which include penetration, spray cone angle, and core length. These characteristics offer a valuable understanding of the overall behavior and evolution of the spray. The second section focuses on microscopic characteristics, covering droplet size and dribbling after the end of injection, and provides in-depth information about the quality of atomization.

6.1. Effects of Injection Pressure on Spray Characteristics

6.1.1. Penetration

Spray tip penetration is defined as the distance along the spray axis from the nozzle exit to the spray's edge. Figure 4 shows the evolution of spray penetration at different injection pressures. It is interesting to note that the spray tip penetration at each injection pressure was measured with a delay, indicating the time elapsed after the injection command. The penetration front reaches the optical limit field of the camera at around 0.15 ms for 700 bar, 0.19 ms for 600 bar, 0.24 ms for 500 bar, 0.29 ms for 400 bar, and 0.41 ms for 300 bar. The figure shows that the spray initially increases linearly due to the increased forces and initial spray momentum, followed by a second phase where the spray penetration stabilizes at 3.9 mm. By comparing the spray penetration at 700 bar and 300 bar, it is observed that the maximum penetration after the delay is reached in 0.1 ms for 700 bar, while for 300 bar, it takes 0.19 ms. At this stage of understanding, the spray behavior depends on initial momentum and the dynamic response to the injection pressure. Zhou et al. [30] studied the various stages of spray tip evolution and identified five distinctive stages: acceleration, first transition, quasi-steady stage, second transition, and finally decelerating. They observed that at each stage, the spray penetration correlates with time as follows: $t^{1.5}$, $t^{0.75}$, $t^{0.5}$, $t^{0.5}$, $(t\text{-injection duration})^{0.25}$. The results show that at higher injection pressures, the penetration length develops fully and more rapidly in a short period due to increased air entrainment. It should also be noted that the spray penetration is influenced by both the nozzle diameter and the needle geometry. The spray penetration equation for the quasi-steady stage and second transition is given by the empirical formula as follows:

$$S \propto \tan\left(\frac{\theta}{2}\right)(d_0)^{0.5}(P)^{0.25}(\rho)^{-0.25}(t)^{0.5}$$

where θ is the cone angle, d_0 is the nozzle diameter, P is the injection pressure, ρ is the gas density, and t is time. According to the equation, spray penetration increases with an increase in the cone angle (larger distribution spray area). In addition, it is observed that the impact of injection pressure on spray penetration is less significant compared to that of the nozzle diameter, as indicated by the lower exponent of 0.25 for pressure and 0.5 for nozzle diameter. Furthermore, during the first phase (acceleration, first transition), spray penetration increases as the velocity of fuel inside the nozzle increases (indicated by a higher Weber number). Generally, a higher fuel velocity indicates a higher non-dimensional Reynolds number (Re), leading to more air being entrained into the spray and increased instability of the spray jet. This enhancement in instability improves atomization and results in better air–fuel mixing.

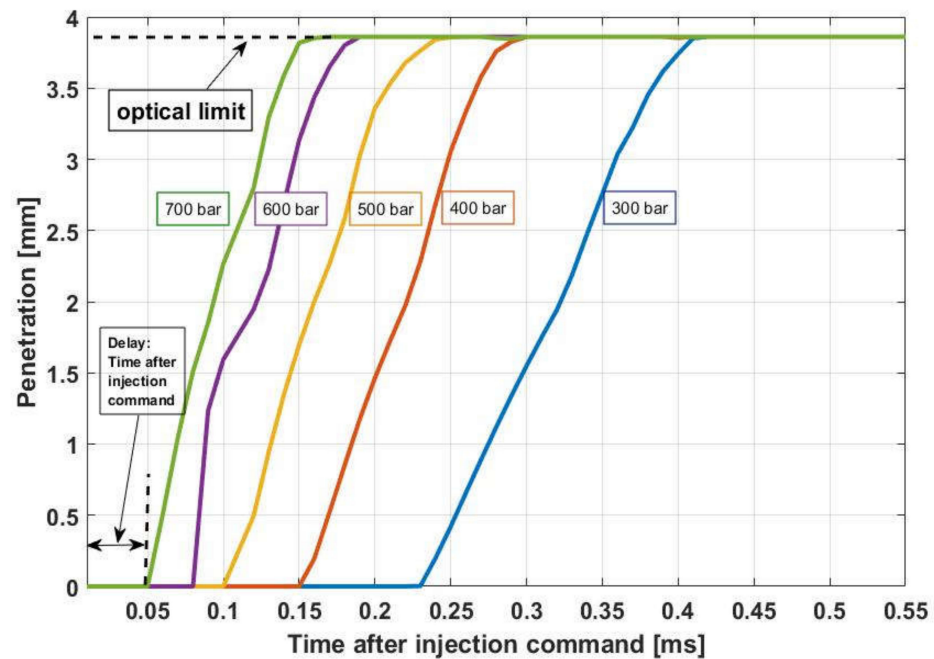


Figure 4. Injection pressure's impact on diesel spray penetration.

6.1.2. Cone Angle

Figure 5 illustrates the spray cone angle at various injection pressures. A closer look at the figure indicates that as the injection pressure increases from 300 bar to 600 bar, the spray cone angle increases from 15° to 19° , indicating a rise of 26.7%. The findings show a narrower cone angle at the start of the injection, due to viscosity, and as we move towards the end of the injection, the cone angle widens [31]. This is attributed to various factors such as needle movement, shearing forces, turbulence within the spray, droplet collisions, and coalescence caused by injection pressures. This pattern of results is consistent with previous research [32]. At the transient stage, the cone angle is observed to be wider compared to the quasi-steady period. This is because of the needle's low lift, which throttles the fuel flow from the needle seat to the orifice. It should be underlined that the configuration of the injector also affects the spray cone angle. The research of Ahmed et al. [33] observed that when the number of ports was reduced from six to two, the cone angle tended to widen. As a final remark, it is also vital to mention that changes in injection pressures between 300 and 400 bar do not significantly affect the cone angle. However, when increasing from 600 to 700 bar, a wider spray cone angle is observed, which can lead to increased air entrainment into the jet, consequently shortening the spray penetration.

The spray cone angle is also influenced by the orifice geometry. In an experimental study conducted by Yu et al. [34], it was found that with an elliptical orifice, the spray angles were wider compared to those of a circular orifice. This is due to the axis-switching effect, which enhances air entrainment and consequently leads to a broader cone angle. In addition, it has been observed that air bubbles within the nozzle contribute to the enhanced thrust of the spray at higher injection pressures. As the pressure increases, the bubbles tend to adhere to the needle. This attachment causes the liquid spray to deflect, resulting in the formation of a wider cone angle [35].

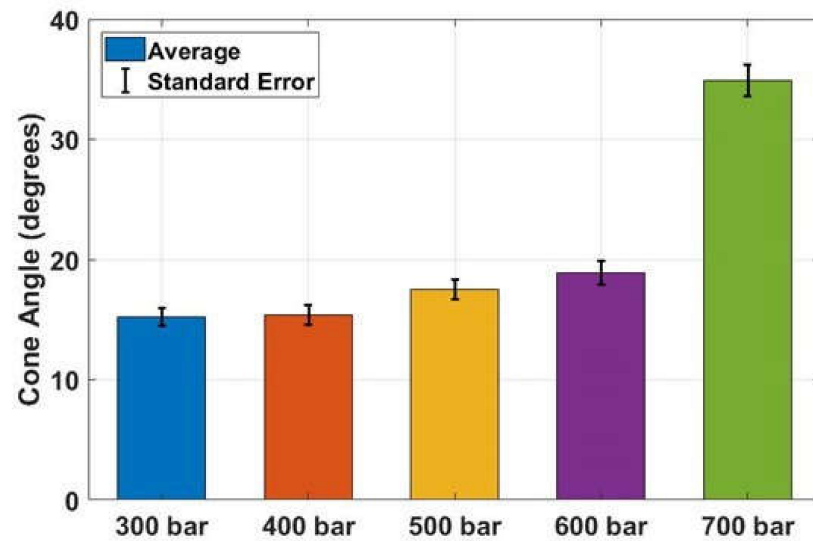


Figure 5. The cone angle of a diesel spray at different injection pressures.

6.1.3. Core Length

This section will point to the temporal evolution of the intact core length under different injection pressures. The red area in Figure 6 represents the unperturbed intermittent region within the spray. Figure 7 illustrates the development of the intact core length under varying injection pressures. The results indicate that at low injection pressures (300 to 500 bar), the intact core length increases by 0.3 mm. At higher injection pressures (500 to 700 bar), the core length increases by 0.14 mm. One interpretation of these findings is that at higher injection pressures, the core region approaches the initial axial velocity of the jet, as given by [36]:

$$V_0 = c \left(2 \frac{\Delta P}{\rho_1} \right)^{\frac{1}{2}} \quad (3)$$

where V_0 and c are the initial axial velocity and the discharge coefficient and ΔP and ρ_1 are the net injection pressure and the liquid density. In addition, the intact core length is influenced by the gas pressure density. According to Reitz et al. [37], the core length increases inversely with the liquid pressure density (with a constant gas density). The equation that describes the core length is as follows:

$$L = \frac{C}{2} d_0 (\rho_1 / \rho)^{\frac{1}{2}} \quad (4)$$

where ρ is the gas density and d_0 is the diameter of the nozzle exit hole. It is clear from Equation (4) that the core length depends on the injector geometry [37]. Therefore, a three-hole injector results in a zero-core length, regardless of the fuel type. However, a single-hole injector typically produces a longer core length and less turbulence along the spray center.

Furthermore, changes in the breakup length, which correspond to variations in jet velocity, are influenced by the nature of the breakup zone [38]. It has been observed that in the turbulent flow region, the jet breakup length increases due to the interaction between the liquid jet and the surrounding gas. This observation further explains the increase in intact core length under higher injection pressures, especially in the turbulent region.

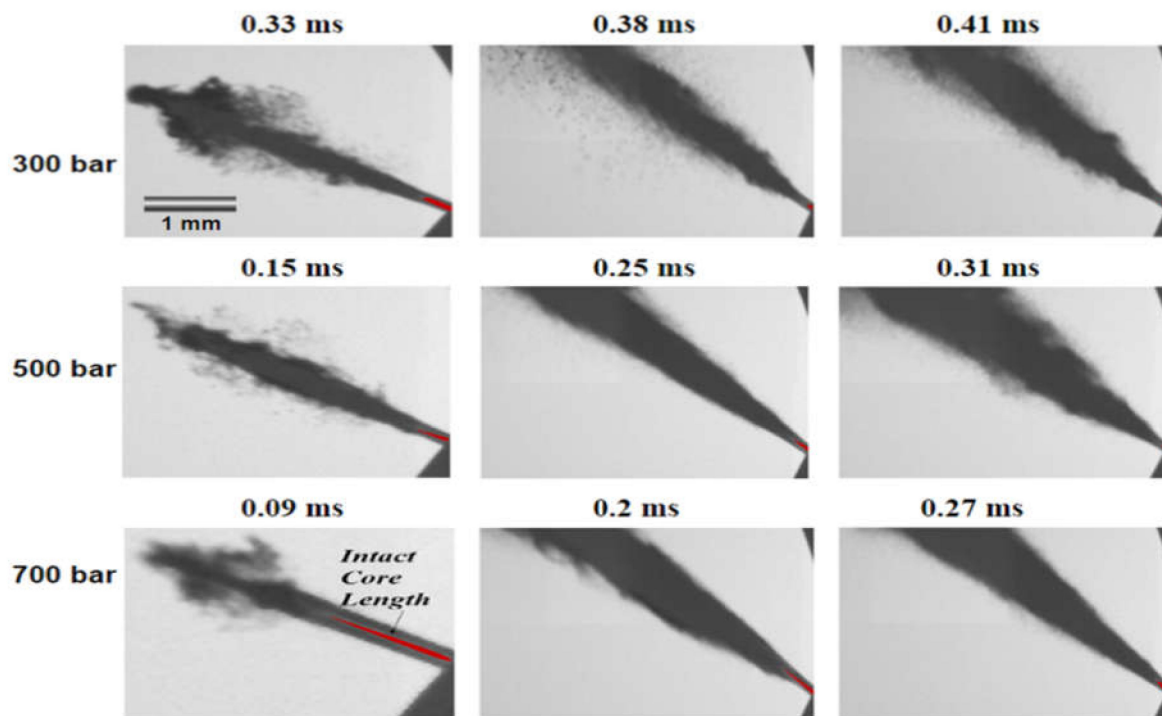


Figure 6. Temporal evolution of intact core length.

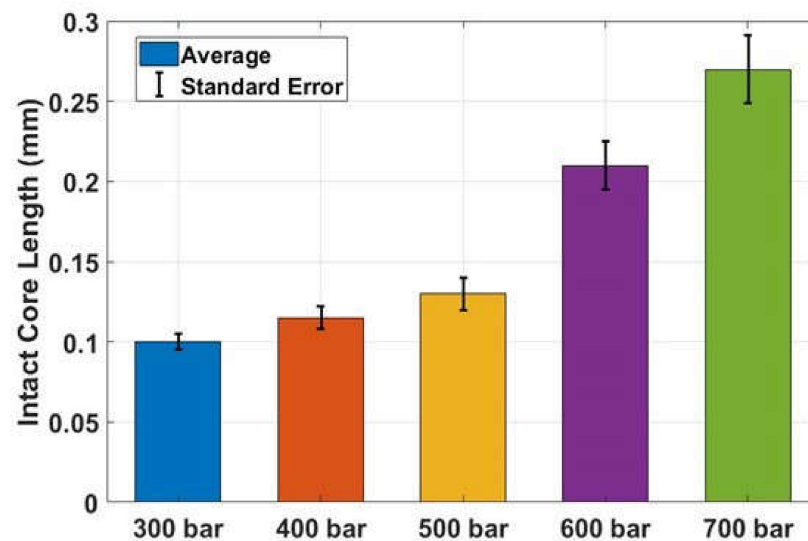


Figure 7. Intact core length of diesel spray at different injection pressures.

6.1.4. Droplet Size

Figure 8 shows the droplet size with various injection pressures. The results indicate that as the injection pressure increases from 300 to 700 bar, the average droplet diameter decreases from 10 to 8.5 μm , which is a reduction of 15%. This decrease is attributed to the greater aerodynamic disturbance at higher pressures, which leads to effective primary atomization. The subsequent re-atomization (secondary atomization) driven by inertial forces also contributes to the formation of smaller droplets. The kinetic energy influences the droplet size distribution at higher pressures, and this trend results in a finer dispersion of fuel droplets [39,40]. This finding aligns with previous research [41] indicating that lower injection pressures result in larger droplets. The surface tension, viscosity, and gas-to-liquid ratio (GLR) were shown to affect the atomization process. As viscosity increases, jet velocity decreases, which leads to the formation of larger droplets. In contrast, a decrease in surface

tension under the conditions of higher temperature and pressure intensifies break-up and favors smaller droplet formation [1]. In general, an increase in injection pressure results in smaller particle formation due to enhanced shearing stresses and turbulence within the flow stream [42]. In a study conducted by Milkvik et al. [43], they examined twin fluid atomizers that were operated with varying gas-to-liquid ratios (GLRs). Their observations revealed that as the GLR increased from 2.5% to 20%, the size of the droplets consistently decreased for all atomizers. Moreover, their findings indicated that in most of these atomizers, the primary break-up process is influenced mainly by air drag resistance. It can be observed that the velocity of the droplets near the spray tip decreases shortly after injection. This decrease is due to the drag force exerted by the air that is stationary in front of the spray tip. Then, as the droplets penetrate further, their velocity increases due to the fuel concentration surpassing the drag force [44].

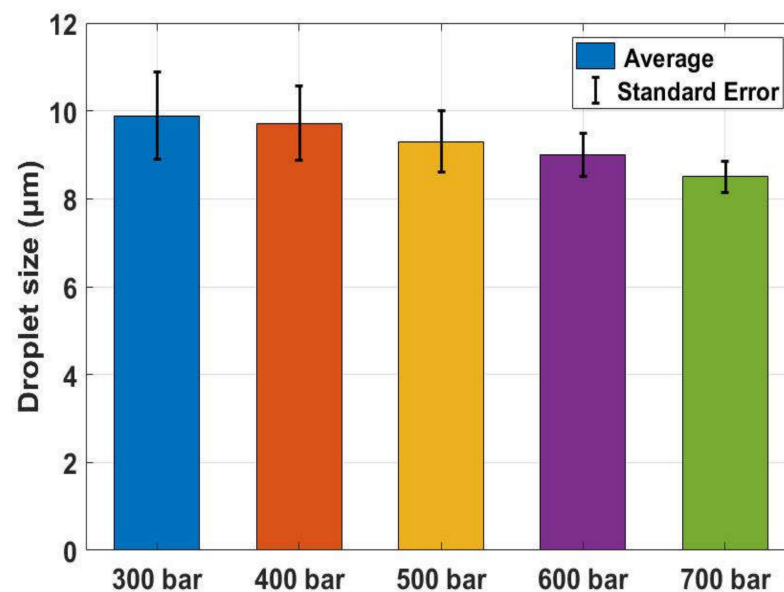


Figure 8. Droplet size distribution across various injection pressure.

6.1.5. Dribbling after the End of Injection (EOI)

Ligament distributions were observed at the end of injection for different injection pressures, as depicted in Figure 9. The smallest ligament size was obtained at the highest pressure (700 bar), at approximately 22 mm^2 . This result is attributed to the enhanced spray atomization and air entrainments [45]. A higher injection pressure promotes the breakup of ligaments into droplets due to the combined effect of capillarity and hydrodynamics [46,47]. Additionally, ligaments are significantly affected by spray shape. As the spray moves downstream, disturbances occur, velocity decreases due to drag and shear forces, causing the spray to lose its spheroid shape and form ligaments [48]. In addition, at the end of injection, careful observation reveals that swirling flows are generated inside the orifices due to the needle valve's eccentric movement, which leads to the fragmentation of the fuel liquid into ligaments [49].

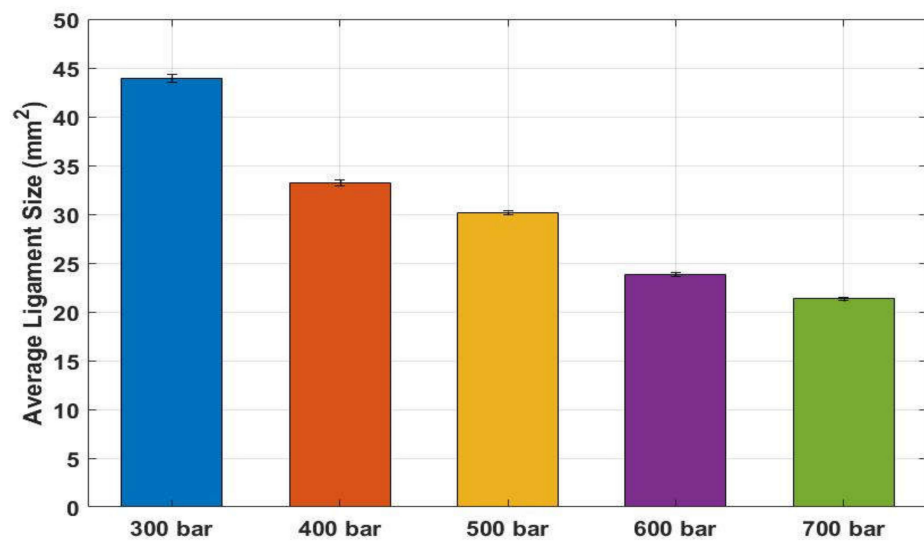


Figure 9. Average ligament size in diesel spray at various injection pressures.

In Figure 10, it is observed that the diameter of the droplets varies due to the distortion of the droplets and their interaction with the turbulent air jet eddies. The collapse of the cavitation bubbles produces ligaments near the nozzle, which over time generate larger droplets. However, the entrainment of ambient air results in the formation of finer droplets at the periphery [50]. One interesting observation is that a higher injection pressure tends to decrease the dribble duration and size. Additionally, it was believed that a faster needle closure speed at higher injection pressures could help to reduce the effects of fuel dribbling [51].

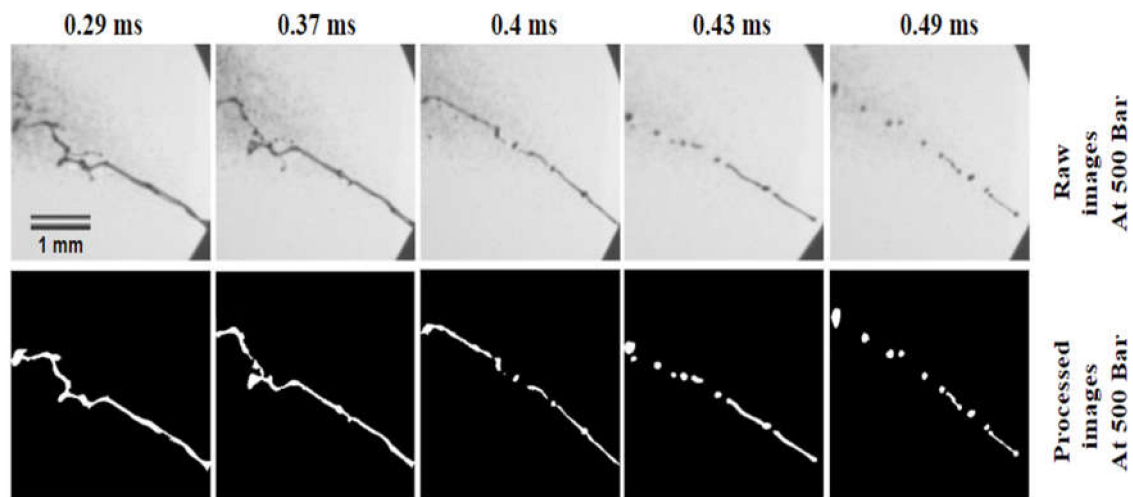


Figure 10. Images of diesel spray ligament breakup after the end of injection.

Furthermore, temperature significantly influences the dribbling at the end of the main injection. It was found that at elevated temperatures, about two to four times more fuel liquid dribbling was generated for all injection pressures. This indicates that temperature has a significant effect on the volume of the fuel dribble. Conversely, as the injection pressure increases, it reduces the volume of dribble due to the decrease in gas density, resulting in less resistance to the flow of fuel ejected from the injector orifice.

7. Conclusions

This paper employed extinction imaging and image processing to experimentally study the macroscopic and microscopic spray behavior under various injection pressures up to 700 bar. Extinction imaging and the projected liquid volume (PLV) were used to describe the diesel spray. The PLV method provides detailed information about the spray characteristics compared to previous approaches that employed Mie scattering and arbitrary thresholding. The effect of injection pressure on spray dynamics is discussed based on the results. The fuel injection system can be adjusted for optimal performance and reduced emissions with these results.

The key conclusions of this study are summarized as follows:

1. A higher injection pressure increased not only the axial but also the radial dispersion of the liquid phase fuel, thus resulting in longer penetration and wider cone angles. This is due to the higher momentum exchange between the liquid spray and ambient air.
2. Droplets formed in the periphery of the spray displayed a decreased diameter from 10 μm to 8.5 μm as the injection pressure increased from 300 bar to 700 bar thanks to enhanced turbulence. This indicates an improved atomization process with a higher injection pressure.
3. Higher injection pressure also showed potential benefits for engine application by reducing dribbling. The dribbling fuel and time were significantly reduced as injection pressure increased. This indicates that the formation of particulate matter emissions can be reduced by an enhanced dribbling process with higher injection pressure.

Author Contributions: Writing—original draft, Y.E.M.; Writing—review & editing, J.H. All authors have read and agreed to the published version of the manuscript.

Funding: This research received no external funding.

Data Availability Statement: Data are contained within the article.

Conflicts of Interest: The authors declare no conflict of interest.

References

1. Lee, S.; Park, S. Experimental study on spray break-up and atomization processes from GDI injector using high injection pressure up to 30 MPa. *Int. J. Heat Fluid Flow* **2014**, *45*, 14–22. [CrossRef]
2. Agarwal, A.K.; Dhar, A.; Gupta, J.G.; Kim, W.I.; Lee, C.S.; Park, S. Effect of fuel injection pressure and injection timing on spray characteristics and particulate size-number distribution in a biodiesel fueled common rail direct injection diesel engine. *Appl. Energy* **2014**, *130*, 212–221. [CrossRef]
3. Chen, P.C.; Wang, W.C.; Roberts, W.L.; Fang, T. Spray and atomization of diesel fuel and its alternatives from a single-hole injector using a common rail fuel injection system. *Fuel* **2013**, *103*, 850–861. [CrossRef]
4. Varde, K.S.; Popa, D.M.; Varde, L.K. Spray Angle and Atomization in Diesel Sprays. 1984. Available online: <https://www.jstor.org/stable/44734209> (accessed on 1 February 2024).
5. Li, G.; Cao, J.; Li, M.; Quan, Y.; Chen, Z. Experimental study on the size distribution characteristics of spray droplets of DME/diesel blended fuels. *Fuel Process. Technol.* **2012**, *104*, 352–355. [CrossRef]
6. Park, S.H.; Cha, J.; Kim, H.J.; Lee, C.S. Effect of early injection strategy on spray atomization and emission reduction characteristics in bioethanol blended diesel fueled engine. *Energy* **2012**, *39*, 375–387. [CrossRef]
7. Das, M.; Sarkar, M.; Datta, A.; Santra, A.K. Study on viscosity and surface tension properties of biodiesel-diesel blends and their effects on spray parameters for CI engines. *Fuel* **2018**, *220*, 769–779. [CrossRef]
8. Lee, C.S.; Park, S.W. An experimental and Numerical Study on Fuel Atomization Characteristics of High-Pressure Diesel Injection Sprays. *Fuel* **2002**, *81*, 2417–2423. [CrossRef]
9. Tsolakis, A. Effects on particle size distribution from the diesel engine operating on RME-biodiesel with EGR. *Energy Fuels* **2006**, *20*, 1418–1424. [CrossRef]
10. Garai, A.; Gangopadhyay, T.; Mukhopadhyay, A.; Sen, S. Spray characterisation of diesel using a hybrid atomizer. *Energy Fuels* **2006**, *20*, 1418–1424. [CrossRef]
11. Agarwal, A.K.; Chaudhury, V.H. Spray characteristics of biodiesel/blends in a high pressure constant volume spray chamber. *Exp. Therm. Fluid Sci.* **2012**, *42*, 212–218. [CrossRef]
12. Rashid, M.S.F.M.; Hamid, A.H.A.; Sheng, O.C.; Ghaffar, Z.A. Effect of inlet slot number on the spray cone angle and discharge coefficient of swirl atomizer. *Procedia Eng.* **2012**, *41*, 1781–1786. [CrossRef]

13. Nagaoka, M.; Ueda, R.; Masuda, R.; Von Berg, E.; Tatschl, R. Modeling of Diesel Spray Atomization Linked with Internal Nozzle Flow. 2011. Available online: https://www.tytlabs.co.jp/en/review/issue/files/422_073nagaoka.pdf (accessed on 1 February 2024).
14. Varde, K.S. Spray Cone Angle and its Correlation in a High Pressure Fuel Spray. *Can. J. Chem. Eng.* **1985**, *63*, 183–187. [[CrossRef](#)]
15. Sovani, S.D.; Chou, E.; Sojka, P.E.; Gore, J.P.; Eckerle, W.A.; Crofts, J.D. High Pressure Effervescent Atomization: Effect of Ambient Pressure on Spray Cone Angle. *Fuel* **2001**, *80*, 427–435. [[CrossRef](#)]
16. Jia, T.M.; Yu, Y.S.; Li, G.X. Experimental investigation of effects of super high injection pressure on diesel spray and induced shock waves characteristics. *Exp. Therm. Fluid Sci.* **2017**, *85*, 399–408. [[CrossRef](#)]
17. Gülder, Ö.L.; Smallwood, G.J.; Snelling, D.R. Diesel Spray Structure Investigation by Laser Diffraction and Sheet Illumination. *J. Engines* **1992**, *101*, 1046–1053.
18. Han, J.-S.; Lu, P.-H.; Xie, X.-B.; Lai, M.-C.; Henein, N.A. Investigation of Diesel Spray Primary Break-up and Development for Different Nozzle Geometries. *J. Engines* **2002**, *111*, 2528–2548. Available online: <https://www.jstor.org/stable/44743268> (accessed on 1 February 2024).
19. Turner, M.R.; Sazhin, S.S.; Healey, J.J.; Crua, C.; Martynov, S.B. A breakup model for transient Diesel fuel sprays. *Fuel* **2012**, *97*, 288–305. [[CrossRef](#)]
20. Agarwal, A.; Trujillo, M.F. The effect of nozzle internal flow on spray atomization. *Int. J. Engine Res.* **2020**, *21*, 55–72. [[CrossRef](#)]
21. Kulkarni, A.P.; Megaritis, T.; Ganippa, L.C. Insights on the morphology of air-assisted breakup of urea-water-solution sprays for varying surface tension. *Int. J. Multiph. Flow* **2020**, *133*, 103448. [[CrossRef](#)]
22. Beale, J.C.; Reitz, R.D. Modeling spray atomization with the Kelvin-Helmholtz/Rayleigh-Taylor hybrid model. *At. Sprays* **1999**, *9*, 623–650. [[CrossRef](#)]
23. Hwang, J.; Bae, C.; Patel, C.; Agarwal, A.; Gupta, T. Near Nozzle Flow and Atomization Characteristics of Biodiesel Fuels. In Proceedings of the International Powertrains, Fuels & Lubricants Meeting, Beijing, China, 16–19 October 2017; SAE Technical Paper; Volume 01.
24. Roth, A.; Frantz, D.; Chaze, W.; Corber, A.; Berrocal, E. High-speed imaging database of water jet disintegration Part I: Quantitative imaging using liquid laser-induced fluorescence. *Int. J. Multiph. Flow* **2021**, *145*, 103641. [[CrossRef](#)]
25. Moon, S.; Huang, W.; Li, Z.; Wang, J. End-of-injection fuel dribble of multi-hole diesel injector: Comprehensive investigation of phenomenon and discussion on control strategy. *Appl. Energy* **2016**, *179*, 7–16. [[CrossRef](#)]
26. Suh, H.K.; Lee, C.S. Effect of cavitation in nozzle orifice on the diesel fuel atomization characteristics. *Int. J. Heat Fluid Flow* **2008**, *29*, 1001–1009. [[CrossRef](#)]
27. Koci, C.; Dempsey, A.; Nudd, J.; Knier, B. Understanding Hydrocarbon Emissions in Heavy Duty Diesel Engines Combining Experimental and Computational Methods. *SAE Int. J. Engines* **2017**, *10*, 1093–1109. [[CrossRef](#)]
28. Pos, R.; Avulapati, M.; Wardle, R.; Cracknell, R.; Megaritis, T.; Ganippa, L. Combustion of ligaments and droplets expelled after the end of injection in a multi-hole diesel injector. *Fuel* **2017**, *197*, 459–466. [[CrossRef](#)]
29. Cha, Y.; Kim, S. PDE-based Interpolation Methods for Image Super Resolution. In Proceedings of the Future Generation Communication and Networking (FGCN 2007), Jeju, Republic of Korea, 6–8 December 2007.
30. Zhou, X.; Li, T. Modeling of the entire processes of diesel spray tip penetration including the start- and end-of-injection transients. *J. Energy Inst.* **2021**, *98*, 271–281. [[CrossRef](#)]
31. Chang, C.T.; Farrell, P.V. A Study on the Effects of Fuel Viscosity and Nozzle Geometry on High Injection Pressure Diesel Spray Characteristics. *J. Engines* **1997**, *106*, 558–567. Available online: <https://www.jstor.org/stable/44730701> (accessed on 1 February 2024).
32. Mithun, M.G.; Koukouvinis, P.; Gavaises, M. Numerical simulation of cavitation and atomization using a fully compressible three-phase model. *Phys. Rev. Fluids* **2018**, *3*, 064304. [[CrossRef](#)]
33. Hamid, A.; Hussein, A.; Atan, R.; Rashid, H. Spray cone angle and air core diameter of hollow cone swirl rocket injector. *IIUM Eng. J.* **2011**, *12*. [[CrossRef](#)]
34. Yu, S.; Yin, B.; Deng, W.; Jia, H.; Ye, Z.; Xu, B.; Xu, H. Experimental study on the spray characteristics discharging from elliptical diesel nozzle at typical diesel engine conditions. *Fuel* **2018**, *221*, 28–34. [[CrossRef](#)]
35. Bao, J.; Wang, H.; Wang, R.; Wang, Q.; Di, L.; Shi, C. Comparative experimental study on macroscopic spray characteristics of various oxygenated diesel fuels. *Energy Sci. Eng.* **2023**, *11*, 1579–1588. [[CrossRef](#)]
36. Ming, Z.; Liu, B.; Zhang, X.; Wen, M.; Liu, H.; Cui, Y.; Ye, Y.; Wang, C.; Jin, C.; Yusuf, A.A.; et al. Study of methanol spray flame structure and combustion stability mechanisms by optical phenomenology and chemical kinetics. *Fuel Process. Technol.* **2023**, *252*, 252107947. [[CrossRef](#)]
37. Reitz, R.D.; Diwakar, R. Structure of High-Pressure Fuel Sprays. 1987. Available online: <https://www.sae.org/publications/technical-papers/content/870598/> (accessed on 1 February 2024).
38. Arai, M.; Shimizu, M.; Hiroyasu, H. Break-up length and spray angle of high speed jet. In Proceedings of the 3rd International Conference on Liquid Atomisation and Spray Systems, London, UK, 8–10 July 1985.
39. Han, D.; Wang, C.; Duan, Y.; Tian, Z.; Huang, Z. An experimental study of injection and spray characteristics of diesel and gasoline blends on a common rail injection system. *Energy* **2014**, *75*, 513–519. [[CrossRef](#)]
40. Farrell, P.V.; Chang, C.T.; Su, T.F. High Pressure Multiple Injection Spray Characteristics. *SAE Trans.* **1996**, *105*, 1271–1280.

41. Liu, X.; Xue, R.; Ruan, Y.; Chen, L.; Zhang, X.; Hou, Y. Effects of injection pressure difference on droplet size distribution and spray cone angle in spray cooling of liquid nitrogen. *Cryogenics* **2017**, *83*, 57–63. [[CrossRef](#)]
42. Manin, J.; Bardi, M.; Pickett, L.M.; Dahms, R.N.; Oefelein, J.C. Microscopic investigation of the atomization and mixing processes of diesel sprays injected into high pressure and temperature environments. *Fuel* **2014**, *134*, 531–543. [[CrossRef](#)]
43. Mlkvik, M.; Stähle, P.; Schuchmann, H.P.; Gaukel, V.; Jedelsky, J.; Jicha, M. Twin-fluid atomization of viscous liquids: The effect of atomizer construction on breakup process, spray stability and droplet size. *Int. J. Multiph. Flow* **2015**, *77*, 19–31. [[CrossRef](#)]
44. Doudou, A.; Maslouhi, A. A Macro-Microscopic Investigation of High-Pressure Sprays Injected by a Common Rail System. *J. Mech. Sci. Technol.* **2007**, *21*, 1284–1292. [[CrossRef](#)]
45. Deshmukh, D.; Ravikrishna, R.V. Studies on microscopic structure of diesel sprays under atmospheric and high gas pressures. *Int. J. Spray Combust. Dyn.* **2014**, *6*, 199–220. [[CrossRef](#)]
46. Chatzigiannakis, E.; Jaensson, N.; Vermant, J. Thin liquid films: Where hydrodynamics, capillarity, surface stresses and intermolecular forces meet. *Curr. Opin. Colloid Interface Sci.* **2021**, *53*, 101441. [[CrossRef](#)]
47. Crua, C.; Shoba, T.; Heikal, M.; Gold, M.; Higham, C. High-Speed Microscopic Imaging of the Initial Stage of Diesel Spray Formation and Primary Breakup. In Proceedings of the SAE 2010 Powertrains Fuels & Lubricants Meeting, San Diego, CA, USA, 25–27 October 2010.
48. Crua, C.; Heikal, M.R.; Gold, M.R. Microscopic imaging of the initial stage of diesel spray formation. *Fuel* **2015**, *157*, 140–150. [[CrossRef](#)]
49. Gavaises, M.; Murali-Girija, M.; Rodriguez, C.; Koukouvinis, P.; Gold, M.; Pearson, R. Numerical simulation of fuel dribbling and nozzle wall wetting. *Int. J. Engine Res.* **2022**, *23*, 132–149. [[CrossRef](#)]
50. Bae, C.; Kang, J. The structure of a break-up zone in the transient diesel spray of a valve-covered orifice nozzle. *Int. J. Engine Res.* **2006**, *7*, 319–334. [[CrossRef](#)]
51. Gong, H.; Huang, W.; Gao, Y.; Wang, J.; Arioka, A.; Sasaki, Y. End-of-injection fuel dribbling dynamics of multi-hole GDI injector. *Fuel* **2022**, *317*, 123406. [[CrossRef](#)]

Disclaimer/Publisher’s Note: The statements, opinions and data contained in all publications are solely those of the individual author(s) and contributor(s) and not of MDPI and/or the editor(s). MDPI and/or the editor(s) disclaim responsibility for any injury to people or property resulting from any ideas, methods, instructions or products referred to in the content.